System Characterization of RiceWrist-S: a Forearm-Wrist Exoskeleton For Upper Extremity Rehabilitation

Ali Utku Pehlivan, *Student Member, IEEE,* Chad Rose, *Student Member, IEEE,*
Marcia K. O'Malley, *Member, IEEE*

***Abstract*— Rehabilitation of the distal joints of the upper extremities is crucial to restore the ability to perform activities of daily living to patients with neurological lesions resulting from stroke or spinal cord injury. Robotic rehabilitation has been identified as a promising new solution, however, much of the existing technology in this field is focused on the more proximal joints of the upper arm. A recently presented device, the RiceWrist-S, focuses on the rehabilitation of the forearm and wrist, and has undergone a few important design changes. This paper first addresses the design improvements achieved in the recent design iteration, and then presents the system characterization of the new device. We show that the RiceWrist-S has capabilities beyond other existing devices, and exhibits favorable system characteristics as a rehabilitation device, in particular torque output, range of motion, closed loop position performance, and high spatial resolution.**

***Index Terms*— Exoskeletons, serial mechanisms, haptic interface design, stroke rehabilitation, spinal cord injury rehabilitation.**

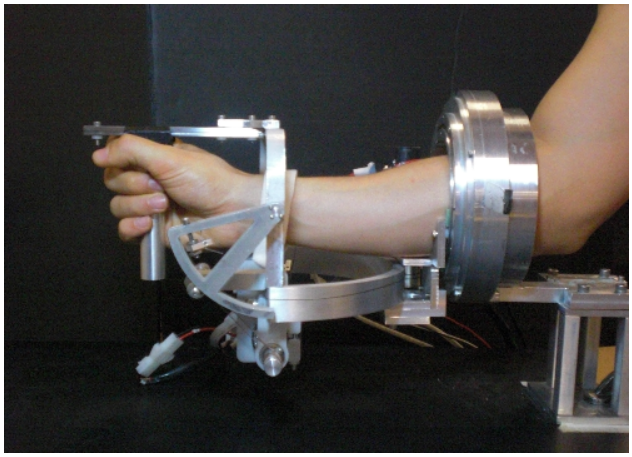

Fig. 1. RiceWrist-S – Forearm and wrist exoskeleton for stroke and spinal cord injury (SCI) rehabilitation.

I. Introduction

In the United States, about 795,000 people suffer a stroke each year. Stroke, the leading cause of long-term disability, has a significant social and economic impact with an estimated $38.6 billion yearly cost [1]. There are approximately 12,000 incidences of Spinal Cord Injury (SCI) in the United States each year [2] with an estimated total yearly direct and indirect costs of $14.5 billion and $5.5 billion, respectively [3]. Due to the large need for rehabilitation and limitations of classical rehabilitation techniques, interest in robotic rehabilitation has increased greatly in recent years.

Clinical studies investigating robotic rehabilitation protocols support the idea of employing these devices in treatment of stroke and SCI patients in order to further induce brain and spinal cord plasticity and improve patient outcomes. Nearly all the activities of daily living (ADL), such as eating, drinking, cleaning, dressing, etc., involve distal upper extremity movement and a certain level of manual dexterity. In order for a stroke or SCI patient to regain the ability to perform ADL, effective rehabilitation of the upper limbs, especially the distal joints, is required. This need is very acute, as it is common for as little as 12% of stroke patients to report no difficulty using their affected hand and 38% to report major difficulty 3 months after their stroke [4].

This project was supported in part by Mission Connect, a project of the TIRR Foundation, and by NSF grant CNS-1135916. The authors are in the Mechatronics and Haptic Interfaces Laboratory, Department of Mechanical Engineering and Materials Science, Rice University, Houston, TX 77005 (e-mails: aliutku@rice.edu, cgr2@rice.edu, omalleym@rice.edu)

In order to facilitate effective rehabilitation of the wrist, an exoskeleton needs to possess: i) a functional workspace that matches healthy human capabilities [5], ii) the ability to apply torques to specific joints [6], and to quantitatively evaluate rehabilitation and pharmacological treatment effects [7], iii) good backdriveability and backlash-free operation [8], and iv) advanced control capabilities [9]. End-effector based robots, such as the MIT-MANUS [10] and Mirror Image Movement Enabler (MIME) [11] possess a large functional workspace, but do not have the capability to apply torques to specific joints or quantitatively evaluate patients like exoskeleton based robots, such as the 5 DOF MAHI Exoskeleton [12], 5 DOF Rupert [13], 6 DOF ARMin [14] and 7 DOF CADEN-7 [15]. However, there is still a need for devices for wrist rehabilitation, and therefore the RiceWrist-S (Fig.1), first presented in detail in [16] (Fig. 2(b)), was designed. This first iteration of the RiceWrist-S mainly addresses the design shortcomings of RiceWrist [17], a serial-in-parallel mechanism, which was designed by our group. In this paper, we will present the mechanical design modifications carried out over previous design of RiceWrist-S and show the system characterization of this new device (Fig. 2(c)). The improvements due to these design modifications will be presented via comparing the system with the first iteration [16]. The system characteristics will also be compared with a same purpose device [18].

978-1-4673-6024-1/13/$31.00 ©2013 IEEE

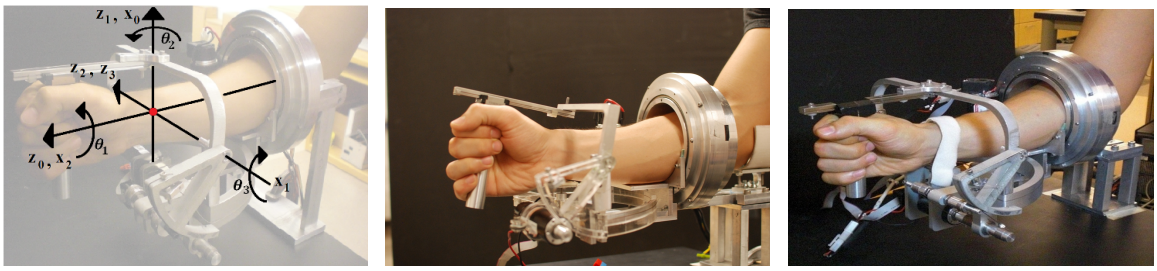

(a) (b) (c)

Fig. 2. (a) Kinematic structure of RiceWrist-S, a 3-DOF serial RRR mechanism. (b) The previous design. (c) The new design introduces considerable design improvements over previous design.

II. Design Details

RiceWrist-S is a 3 DOF, electrically actuated, grounded forearm-wrist exoskeleton. The system is a serial RRR manipulator, the kinematic structure of which is depicted in Fig. 2(a). RiceWrist-S is capable of actuating the user's forearm pronation/supination (PS), wrist flexion/extension (FE), wrist radial/ulnar deviation (RU) DOFs separately. In addition to the actuated DOFs, the system employs a passive linear degree of freedom on the handle coupling in order to keep the user's wrist in an anatomically natural posture.

In order to ensure zero backlash and low friction on the FE and RU joints, the RiceWrist-S utilizes cable drive transmissions, while the PS joint employs a frameless, brushless motor with direct drive.

The mechanical design of the device presented in this work introduces considerable design improvements in both RU and FE joint over the device introduced in [16]. The modifications, rationale, and results of the modifications are presented in detail below, grouped under RU and FE joint subsections.

A. RU Joint

Different from the previous design, the new exoskeleton employs a cable routing system to transmit the actuation on the RU joint. The actuation is transferred from the motor shaft to the transmission shaft via two steel cables (see Fig. 3). The method, described in [19], requires first winding cables in opposite directions, then fixing them on both the motor shaft and the transmission shaft. Pretension has to be applied to both cables in order to achieve sufficient stiffness.

In order to pretension the cables, a precision threaded steel transmission rod was coupled with two threaded aluminum cylinders. The cables, which are fixed on the motor shaft from one end, are fixed to these two cylinders, rather than to the transmission shaft itself. So, by screwing the cylinders away from each other, pretension can be applied to the cables. Two nuts are used for each cylinder to prevent them from loosening.

One end of the transmission shaft is used as a capstan spool. The capstan arc, coupled to the device handle, is driven by means of a cable drive system (Fig. 3). We used a Maxon RE-30 brushed DC motor for the actuation and a CPT Avago 5540 HEDS optical encoder with 500 counts per revolution for position sensing at the RU joint (see Table I).

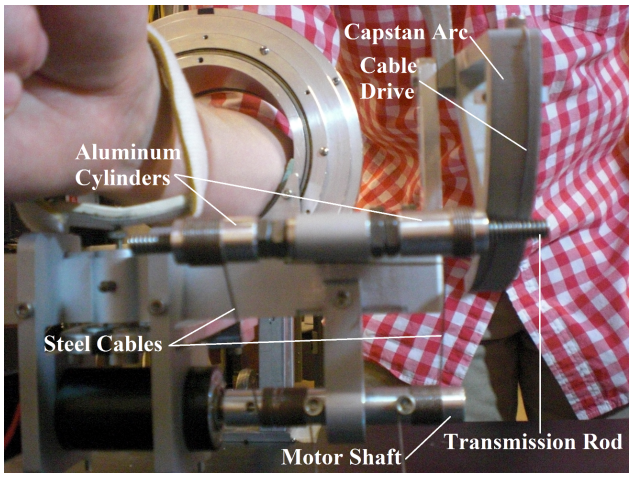

Fig. 3. RU joint cable routing detailed demonstration.

The main benefit of the cable routing system is that it enables us to place the RU joint actuator exactly below the FE rotation axis, decreasing the inertia of the mechanism considerably compared to the previous design.

In the previous design, the capstan arc was driven by the threaded spool which is attached to the motor shaft (Fig. 2(b)). Because of the thickness of the motor shaft, the spool had to have a certain thickness and we could not achieve a larger transmission ratio than 1:12.5. In the new design we could specify the thickness of the transmission shaft independent from any factor, and achieved a 1:24 transmission ratio. The increase of the transmission ratio provided both higher torque outputs and better sensor resolution (see Table I and II). One potential problem regarding this design is the difficulty of cable installation.

B. FE Joint

The placement of the actuators is very important for keeping the inertia of the device as low as possible, in turn resulting in better backdrivability. In the previous design, we placed the FE actuator tangentially to the opening of the PS actuator in order to keep the distance of the FE actuator as close as possible to the PS rotation axis. Another consideration for the placement of the FE actuator was that a cable drive system was employed for the transmission, and the spool, which was attached to the motor shaft, had to be

TABLE I

SENSOR AND ACTUATOR SPECIFICATIONS

Joint	Actuator	Transmission	Sensor	Sensor Resolution
Forearm Pronation/Supination	Applimotion 165-A-18	Direct-Drive	MicroE Mercury 1500	0.002°
Wrist Flexion/Extension	Maxon RE-40 (148877)	Cable-Drive (1:18)	Avago HEDS 5540	0.01°
Wrist Radial/Ulnar Dev.	Maxon RE-30 (310009)	Cable-Drive (1:24)	Avago HEDS 5540	0.0075°

TABLE II

ACHIEVABLE JOINT RANGES OF MOTION (ROM) AND MAXIMUM CONTINUOUS JOINT TORQUE OUTPUT VALUES FOR RICEWRIST-S.THE VALUES GIVEN IN PARENTHESIS IN THE TORQUE COLUMN SHOWS THE CAPABILITY OF THE OLD DESIGN. THE REQUIRED ROM AND TORQUE VALUES FOR 19 (ADL) AS EXTRACTED FROM [15] ARE ALSO GIVEN FOR COMPARISON.

Joint	ADL		RiceWrist-S	
	ROM (deg)	Torque (Nm)	ROM (deg)	Torque (Nm)
Forearm Pronation/Supination	150	0.06	180	1.69 (1.69)
Wrist Flexion/Extension	115	0.35	130	3.37 (2.80)
Wrist Radial/Ulnar Dev.	70	0.35	75	2.11 (1.10)

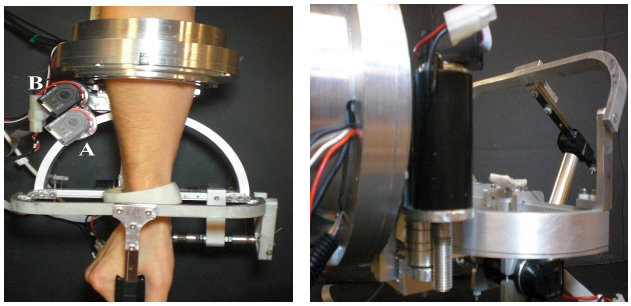

(a) (b)

Fig. 4. (a) The shaded motor is a representative demonstration of the approximate placement of the FE actuator in the previous design. The actuator is moved from A to B, in order to install another support for the device handle and get a more rigid device. (b) An idle pulley mechanism is used to relocate the actuator.

as close to the capstan arc as possible. These two constraints decided the thickness of the spool, hence we could not apply more than 1:15 transmission ration. Also, because the motor was placed closely to the capstan arc, installation of a second support for the device handle was not possible, which was affecting the rigidity of the device negatively. In the new design, we kept the distance of the flexion/extension actuator same as the previous design, however, by employing an idle pulley mechanism (Fig. 4(b)) we could place the actuator further back (Fig. 4(a)). By this way we could install another support for the device handle and get a more rigid device. Also, the freedom of choosing the placement of the actuator enabled us to increase the transmission ratio to 1:18 (see Table II).

We utilized a Maxon RE-40 brushed DC motor with a CPT Avago 5540 HEDS optical encoder with 500 counts per revolution for actuation and sensing , and employed a steel cable for the cable drive transmission system. In order to prevent any slippage, the cable is wrapped around both the idle pulley and the spool three times.

III. DEVICE MODELING AND CHARACTERIZATION

In this section, we will examine the kinematics of the RiceWrist-S, and present the experimentally determined characterization of the device, including the spatial resolution, static friction, bandwidth, viscous friction coefficient and inertial elements. This system characterization is made in order to evaluate the device's potential for rehabilitation use.

A. Kinematics

The RiceWrist-S is a pure rotational manipulator, we are interested in the orientation of the user's wrist-forearm. In the neutral position, which is shown in the Fig. 2(a), z_0, z_1 and z_2 coincides with the user's PE, FE and RU rotation axes respectively. Frame $\{1\}$ is coincided with frame $\{0\}$, then rotated $-\frac{\pi}{2}$ radians around x_0, and the rotation θ_1 around z_0 corresponds to the user's rotation around his/her PS rotation axis. Similarly, frame $\{2\}$ coincides with frame $\{1\}$, then rotated $\frac{\pi}{2}$ radians around x_1, and the rotation θ_2 around z_1 corresponds to user's rotation around the FE rotation axis. Frame $\{3\}$ coincides with frame $\{2\}$ and the rotation around z_2 corresponds to the RU rotation of the user. The Denavit-Hartenberg parameters of the system can be given as follows:

TABLE III

LINK PARAMETERS FOR THE FOREARM AND WRIST JOINTS

Joint	rot(x)	tr(x)	rot(z)	tr(z)
Forearm	$-\frac{\pi}{2}$	0	θ_1	0
Wrist F/E	$\frac{\pi}{2}$	0	θ_2	0
Wrist R/U	0	0	θ_3	0

The corresponding transformation matrix from frame $\{3\}$ to frame $\{0\}$ is

$$ {}^0T_3 = \begin{bmatrix} c1c2c3-s1s3 & -c1c2s3-s1c3 & c1s2 & 0 \\ s1c2c3+c1s3 & -s1c2s3+c1c3 & s1s2 & 0 \\ -s2c3 & s2s3 & c2 & 0 \\ 0 & 0 & 0 & 1 \end{bmatrix} \quad (1) $$

In the above equation, while s and c stands for sine and cosine, 1,2 and 3 stand for θ_1, θ_2 and θ_3, respectively.

The Jacobian relating the link velocities to the end effector angular velocities is given as

$$J = \begin{bmatrix} 0 & -s1 & c1s2 \\ 0 & c1 & s1s2 \\ 1 & 0 & c2 \end{bmatrix} \quad (2)$$

The kinematic structure shows that, singularity occurs when z_0 and z_2 are aligned, i.e., when $\theta_2 = \pm\frac{\pi}{2}$. The θ_2 (which corresponds to FE rotation) mechanically constrained to be between $\pm 65°$(1.13 rad) (see Table II), hence the device is singularity free.

B. Spatial Resolution

We calculated the spatial resolution of the RiceWrist-S by using the sensor resolutions and the Jacobian of the device. Any instantaneous change in the joint space causes an instantaneous change in the task space which are related by the device's Jacobian. In order to quantify the spatial resolution, we created approximately 35,000 scenarios in which to compute the effect of the smallest instantaneous change detectable in the joint space on the end effector. The worst-case result of these scenarios in any DOF was a spatial resolution of 2.1816 $\times 10^{-4}$ radians.

C. Device Characterization

The friction and inertia characteristics of every joint of the device are obtained by investigating simple ramp and step inputs to the system in a similar way presented in [20].

A ramp position command which stays constant for 2 seconds, and ramps up (or down) 5° (0.088 radians) in 2 seconds is sent to the system for each joint separately. The command starts from 0°, goes up to 45° (25° for RU joint) goes down to -45° (-25° for RU joint) and comes back to 0°. In this way, we obtained static friction values for different locations. In order to eliminate gravitational effects as much as possible during the tests, the device was brought to a configuration at which the axis of rotation of the joint being tested was parallel to the direction of gravity, and the handle of the device is fixed and the other two joints are locked in the neutral position. The corresponding actuator is programmed as a spring, and the forces applied at zero velocity is recorded. Fig. 5(a) presents the torque values commanded to the RU actuator while the velocity is zero. The spikes occur at the instant movement is initiated, when the device overcomes static friction. The maximum static friction values are presented in Table IV. The values are less than 13% of the continuous torque output values for every joint.

The dynamical properties of the device were determined by investigating the response of the system to a step position command. We adopted the logarithmic decrement method presented in [21], which isolates the inertial and viscous effects responsible for the exponential decay of the free vibration of the system. A position input which steps up from 0° to 25° (0.436 radians) (45° for PS joint), and steps back to 0° (Fig. 6) is commanded. Table III presents the static friction coefficients, viscous damping coefficient and inertial element values.

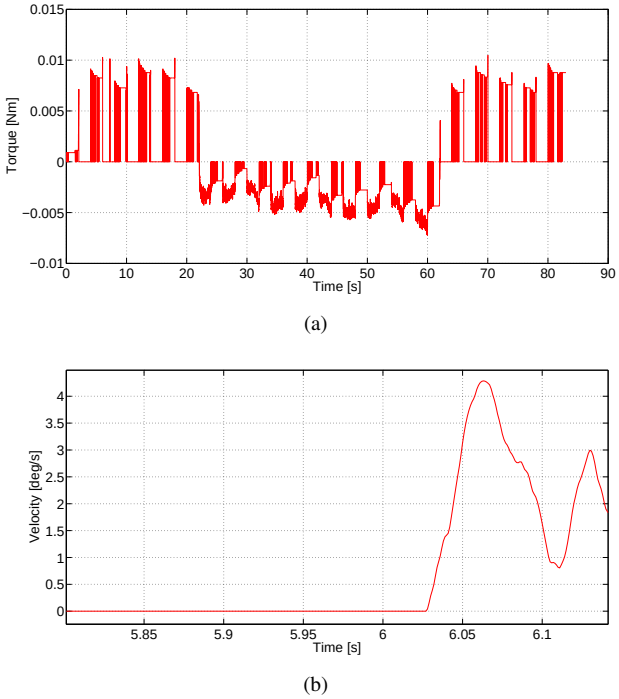

Fig. 5. (a) The commanded torque input to the RU joint actuator at zero velocity. The spikes occur at the movement initiation instances. (b) The close up view of RU joint velocity at one of the ramping up initiation instances. The desired trajectory imposes movement initiation at 6th second, but the movement starts after the static friction is overcame.

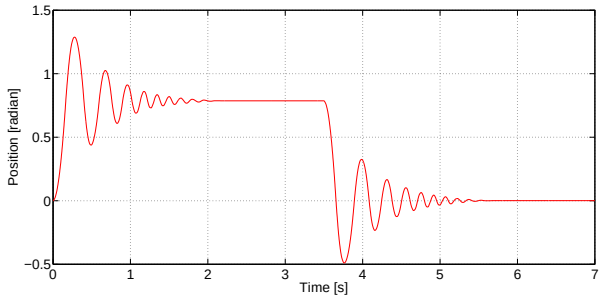

Fig. 6. The response at the PS joint to a step position command with a proportional control. The actuator is programmed to act as a spring with spring constant of 54.4 $\frac{Nm}{rad}$.

D. Closed Loop Position Bandwidth

Depending on the intended control strategy, the control implementations of robotic devices might employ closed loop position control. In order to examine the position control performance of the device we identified the closed loop position bandwidth by tracking a sine position input with PD controller for every DOF separately. The amplitude of the input signal was set to 10° (0.175 rad) and the frequency was increased gradually. The Bode plots for every DOF is shown in Fig. 7. We observed approximately 3.6 Hz, 6 Hz ,and 8.3 HZ bandwidths for PS, FE, and RU DOF respectively. These

TABLE IV

DEVICE CHARACTERISTICS. THE VALUES IN THE PARENTHESIS IN THE FIRST TWO COLUMNS ARE THE RELATED VALUES FOR THE DEVICE DESCRIBED IN [18], AND THEY ARE GIVEN FOR COMPARISON.

Joint	**Static Friction** (Nm)	**Inertia** $(kg.m^2)$	**Viscous Coeff.** $(\frac{Nm.s}{rad})$	**CL Position Bandwidth** (Hz)
Forearm Pronation/Supination	0.221 (0.29)	0.157 (0.0058)	0.428	3.5
Wrist Flexion/Extension	0.198 (0.075)	0.0054 (0.0040)	0.085	6
Wrist Abduction/Adduction	0.211 (0.075)	0.0048 (0.0031)	0.135	8.3

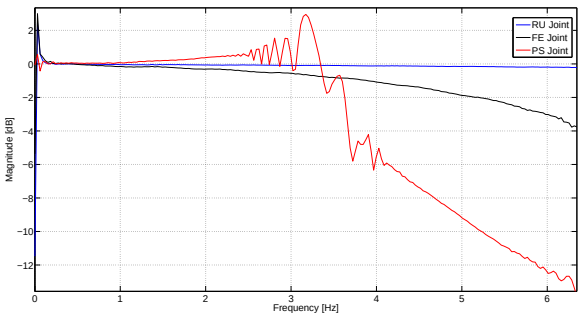

Fig. 7. Bode plot for PS, FE and RU joints. The bandwidth values are 3.6 Hz, 6 Hz ,and 8.3 Hz respectively.

bandwidth values are comparable to the human movement capability, which is desirable feature for robotic rehabilitation devices.

IV. DISCUSSION

In this paper, we presented the system characterization of the RiceWrist-S, an exoskeleton for stroke and SCI patient rehabilitation. By modifying the previous design, the RiceWrist-S was able to provide higher torque output capabilities, lower inertia and a more robust system than the previous design. The presented system characterization of this novel device shows that the RiceWrist-S has the potential to conduct state-of-the-art rehabilitation regimens. The RiceWrist-S possesses the ability to cover more than the required workspace for ADL. The device provides comparable system characteristics to an existing, same purpose device [18]. Although the static friction values are relatively higher for FE and RU joints, the high continuous torque values that device can provide, enables to overcome in software the high friction. Additionally, these high torque capabilities ,above those required for matching the values required for ADL, enables us to implement a wide range of control algorithms (both assistive and resistive control algorithms).

The kinematic structure of the RiceWrist-S provides advantages in terms of application diversity. The RiceWrist-S, by decoupling the wrist joints, enables implementation of different movements compared to the stated device [18], such as backdriving one of the wrist joints while locking the other wrist joint.

REFERENCES

[1] A. Go, D. Mozaffarian, V. Roger, E. Benjamin, J. Berry, W. Borden, D. Bravata, S. Dai, E. Ford *et al.*, "Heart disease and stroke statistics–2013 update: A report from the American Heart Association," *Circulation*, vol. 127, p. e8, 2013.

[2] Anon., "Spinal cord injury facts and figures at a glance," *National Spinal Cord Injury Statistical Center*, February 2012.

[3] M. Berkowitz, *Spinal cord injury: An analysis of medical and social costs*. Demos Medical Pub, 1998.

[4] P. Duncan, R. Bode, S. Min Lai, S. Perera *et al.*, "Rasch analysis of a new stroke-specific outcome scale: the stroke impact scale1," *Archives of physical medicine and rehabilitation*, vol. 84, no. 7, pp. 950–963, 2003.

[5] A. Schiele and F. C. T. van der Helm, "Kinematic design to improve ergonomics in human machine interaction," *IEEE Transactions on Neural Systems and Rehabilitation Engineering*, vol. 14, no. 4, pp. 456–469, 2006.

[6] J. Klein, S. Spencer, and D. Reinkensmeyer, "Breaking it down is better: Haptic decomposition of complex movements aids in robot-assisted motor learning," *Neural Systems and Rehabilitation Engineering, IEEE Transactions on*, vol. 20, no. 3, pp. 268–275, 2012.

[7] O. Celik, M. K. O'Malley, C. Boake, H. Levin, S. Fischer, and T. Reistetter, "Comparison of robotic and clinical motor function improvement measures for sub-acute stroke patients," in *Proc. IEEE International Conference on Robotics and Automation (ICRA 2008)*, Pasadena, CA, USA, May 2008, pp. 2477–2482.

[8] V. Hayward and K. MacLean, "Do it yourself haptics: Part i," *Robotics & Automation Magazine, IEEE*, vol. 14, no. 4, pp. 88–104, 2007.

[9] E. Wolbrecht, V. Chan, D. Reinkensmeyer, and J. Bobrow, "Optimizing compliant, model-based robotic assistance to promote neurorehabilitation," *Neural Systems and Rehabilitation Engineering, IEEE Transactions on*, vol. 16, no. 3, pp. 286–297, 2008.

[10] H. I. Krebs, N. Hogan, M. L. Aisen, and B. T. Volpe, "Robot-aided neurorehabilitation," *IEEE Trans. Rehab. Eng.*, vol. 6, no. 1, pp. 75–87, 1998.

[11] P. S. Lum, C. G. Burgar, P. C. Shor, M. Majmundar, and M. Van der Loos, "Robot-assisted movement training compared with conventional therapy techniques for the rehabilitation of upper-limb motor function after stroke." *Arch Phys Med Rehabil*, vol. 83, no. 7, pp. 952–9, 2002.

[12] A. Gupta and M. K. O'Malley, "Design of a haptic arm exoskeleton for training and rehabilitation," *IEEE/ASME Transactions on Mechatronics*, vol. 11, no. 3, pp. 280–289, 2006.

[13] T. G. Sugar, J. He, E. J. Koeneman, J. B. Koeneman, R. Herman, H. Huang, R. S. Schultz, D. E. Herring, J. Wanberg, S. Balasubramanian, P. Swenson, and J. A. Ward, "Design and control of RUPERT: a device for robotic upper extremity repetitive therapy," *IEEE Trans. Neural Syst. Rehab. Eng.*, vol. 15, no. 3, pp. 336–346, 2007.

[14] T. Nef, M. Mihelj, G. Kiefer, C. Perndl, R. Muller, and R. Riener, "ARMin-exoskeleton for arm therapy in stroke patients," in *IEEE 10th International Conference on Rehabilitation Robotics (ICORR 2007)*. IEEE, 2008, pp. 68–74.

[15] J. C. Perry, J. Rosen, and S. Burns, "Upper-limb powered exoskeleton design," *IEEE/ASME Transactions on Mechatronics*, vol. 12, no. 4, pp. 408–417, 2007.

[16] A. Pehlivan, S. Lee, and M. O'Malley, "Mechanical design of ricewrist-s: A forearm-wrist exoskeleton for stroke and spinal cord injury rehabilitation," in *Biomedical Robotics and Biomechatronics (BioRob), 2012 4th IEEE RAS & EMBS International Conference on*. IEEE, 2012, pp. 1573–1578.

[17] M. OMalley, A. Sledd, A. Gupta, V. Patoglu, J. Huegel, and C. Burgar, "The ricewrist: A distal upper extremity rehabilitation robot for stroke therapy," in *ASME International Mechanical Engineering Congress and Exposition*, 2006.

[18] H. I. Krebs, B. T. Volpe, D. Williams, J. Celestino, S. K. Charles, D. Lynch, and N. Hogan, "Robot-aided neurorehabilitation: a robot for

wrist rehabilitation," *Neural Systems and Rehabilitation Engineering, IEEE Transactions on*, vol. 15, no. 3, pp. 327–335, 2007.

[19] J. K. Salisbury Jr, W. T. Townsend, D. M. DiPietro, and B. S. Eberman, "Compact cable transmission with cable differential," Sep. 10 1991, uS Patent 5,046,375.

[20] J. R. Celestino, "Characterization and control of a robot for wrist rehabilitation," Master's thesis, Massachusetts Institute of Technology, 2003.

[21] J. Liang and B. Feeny, "Identifying coulomb and viscous friction from free-vibration decrements," *Nonlinear Dynamics*, vol. 16, pp. 337–347, 1998.